Electronic Supplementary Material (ESI) for Journal of Materials Chemistry A.

Supplementary information

On the chemistry and electrochemistry of LiPON

Brecht Put[†‡*], Philippe M. Vereecken[†¶] ,Andre Stesmans[‡]

[‡] Department of Physics, Celestijnenlaan 200D, University of Leuven, 3001 Leuven, Belgium

[†] Imec, Kapeldreef 75, 3001 Leuven, Belgium

[¶] Centre for Surface Chemistry and Catalysis, University of Leuven, Kasteelpark Arenberg 23, 3001 Leuven, Belgium}

[*] brecht.put@imec.be

Fig S1: : I-V curves (potential applied to the metal dot and scanned at a sweep rate of 140 kV/cm.s) of a 200 nm BKM LiPON layer contacted using a 500 µm (diameter) gold metal dot contact on a TiN current collector. Usage of the TiN current collector gives rise to asymmetric breakdown. Constant current plateaus are detected for both positive and negative sweep directions and are also clearly present in the zoom in panel b. The calculated breakdown fields for the BKM LiPON here are 2.2 MV/cm and 0.6 MV/cm for respectively negative and positive sweep directions. These are close to the ones for the Std LiPON (namely -2.5 MV/cm and 0.8 MV/cm).

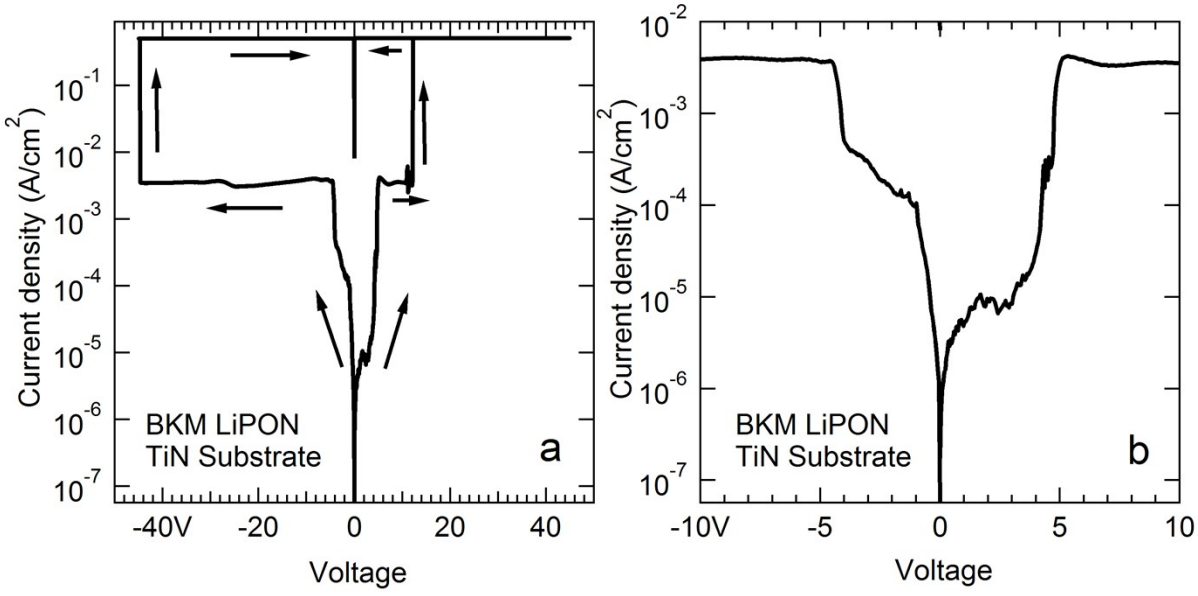

Fig S2: I-V curves (potential applied to the metal dot and scanned at a sweep rate of 140 kV/cm.s) of a 140 nm Std LiPON layer contacted using a 500 µm (diameter) gold metal dot contact on a Pt current collector. Usage of a platinum current collector gives rise to symmetric breakdown. Constant current plateaus are detected for both positive and negative sweep directions and are also clearly present in the zoom in panel b.

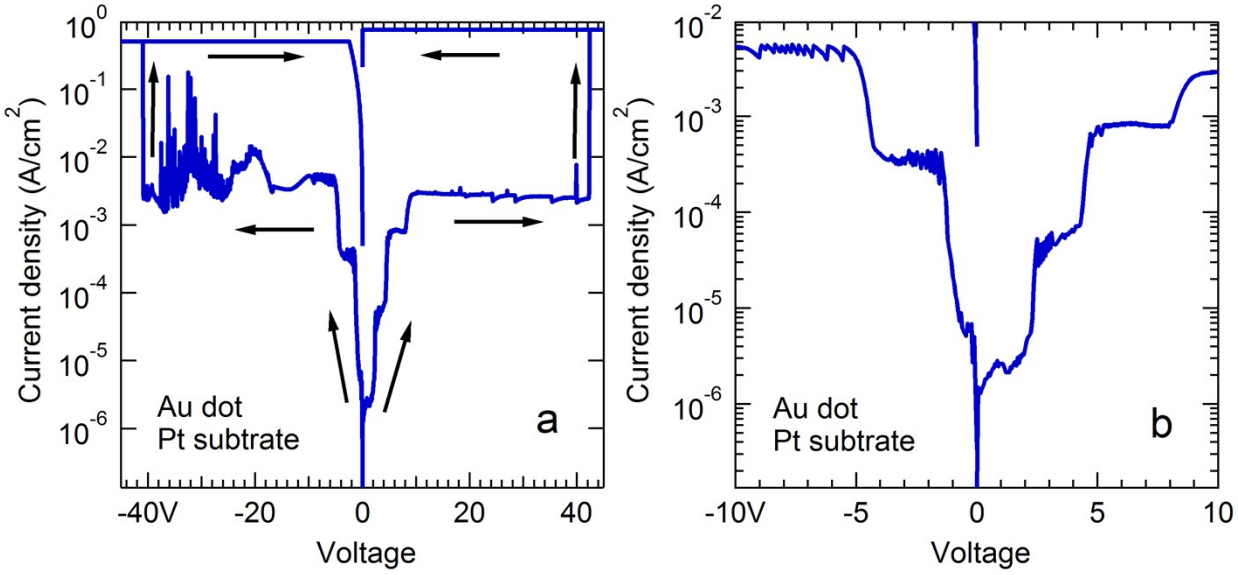

A behavior similar to the three regions detected on TiN is also found for the platinum current collector. Under application of a bias, multiple distinct plateaus are detected in figure S2a. These gradually increase in current and stabilize from 5V onward, at this point again a current density of 3 mA/cm^2 flows. At a potential of 40 V (E_{bd} ~2.8 MV/cm), hard breakdown is registered under positive bias application. When applying a negative sweep, noise is seen starting from approximately -30V which

eventually culminates in hard breakdown (at -40 V or -2.8 MV/cm). This is consolidated by the high current level in the reverse trace.

Reaction	ΔG^0 (kJ/mol)
$2Li_3PO_4 <-> Li_4P_2O_7 + 1/2O_2 + 2Li^+ + 2e^-$	221.0
$2Li_3PO_4 <-> Li_4P_2O_7 + Li_2O$	237.7
$Li_4P_2O_7 <-> 2LiPO_3 + Li_2O$	249.9
$4LiPO_3 <-> P_4O_{10} + 2Li_2O$	814.3
$Li_3PO_4 <-> LiPO_3 + Li_2O$	243.8
$4Li_3PO_4 <-> P_4O_{10} + 6Li_2O$	1789.5
$2Li_4P_2O_7 <-> P_4O_{10} + 4Li_2O$	1314.5

Table T1: Decomposition reactions of LiPON with their corresponding reaction energies

Note that two different values for the standard Gibbs energy of formation for Li_3PO_4 have been reported in literature[1,2]. In the present work, the calculations are based on the value reported by Yokokawa *et al.*[2] since this value agreed best with the reaction energy extracted from the solubility product constant K_{SP}[3].

[1] S.P. Ong, L. Wang, B. Kang, G. Ceder, Li-Fe-P-O2 Phase diagram from first principles calculations, *Chemistry of Materials*, 2008

[2] H. Yokokawa, Thermodynamic stability of sulfide electrolyte/oxide electrode interface in solid-state lithium batteries, Solid state ionics, 2015

[3] CRC Handbook of chemistry and physics, 1975-1976, Ed: R.C. Weast, CRC Press, ISBN: 0-87819-455-X

Reaction	Standard potential U^0 (V)
$2\ Au_2O_3 + 3\ P_4O_{10} + 12e^- + 12\ Li^+ \rightarrow 4\ Au + 12\ LiPO_3$	2.12
$P_4O_{10} + 4\ e^- + 4\ Li^+ + O_2 \rightarrow 4\ LiPO_3$	1.99
$4\ Au_2O_3 + 3\ P_4O_{10} + 24\ e^- + 24\ Li^+ \rightarrow 8\ Au + 6\ Li_4P_2O_7$	1.71
$P_4O_{10} + 8\ e^- + 2\ O_2 + 8\ Li^+ \rightarrow 2\ Li_4P_2O_7$	1.58
$2\ Au_2O_3 + P_4O_{10} + 12\ e^- + 12\ Li^+ \rightarrow 4\ Au + 4\ Li_3PO_4$	1.55
$P_4O_{10} + 12\ e^- + 12\ Li^+ + 3\ O_2 \rightarrow 4\ Li_3PO_4$	1.42
$Au_2O_3 + 6\ LiPO_3 + 6\ e^- + 6\ Li^+ \rightarrow 2\ Au + 3\ Li_4P_2O_7$	1.3
$Au_2O_3 + 3\ LiPO_3 + 6\ e^- + 6\ Li^+ \rightarrow 2\ Au + 3\ Li_3PO_4$	1.27
$Au_2O_3 + 3\ Li_4P_2O_7 + 6\ e^- + 6\ Li^+ \rightarrow 2\ Au + 6\ Li_3PO_4$	1.24
$4\ LiPO_3 + 4\ e^- + O_2 + 4Li^+ \rightarrow 2\ Li_4P_2O_7$	1.17
$2\ LiPO_3 + 4\ e^- + 4\ Li^+ + O_2 \rightarrow 2\ Li_3PO_4$	1.14
$2\ Li_4P_2O_7 + 4\ e^- + 4\ Li^+ + O_2 \rightarrow 4\ Li_3PO_4$	1.11
$2\ TiO_2 + N_2 + 2\ P_4O_{10} + 8\ e^- + 8\ Li^+ \rightarrow 2\ TiN + 8\ LiPO_3$	0.31
$2\ TiO_2 + N_2 + P_4O_{10} + 8\ e^- + 8\ Li^+ \rightarrow 2\ TiN + 2\ Li_4P_2O_7$	-0.1
$6\ TiO_2 + 3\ N_2 + 2P_4O_{10} + 24\ e^- + 24\ Li^+ \rightarrow 6\ TiN + 8\ Li_3PO_4$	-0.25
$2\ TiO_2 + N_2 + 8\ LiPO_3 + 8\ e^- + 8\ Li^+ \rightarrow 2\ TiN + 4\ Li_4P_2O_7$	-0.5
$2\ TiO_2 + N_2 + 4\ LiPO_3 + 8\ e^- + 8Li^+ \rightarrow 2\ TiN + 4\ Li_3PO_4$	-0.53
$2\ TiO_2 + N_2 + 4\ Li_4P_2O_7 + 8\ e^- + 8\ Li^+ \rightarrow 2\ TiN + 8\ Li_3PO_4$	-0.56

Table T2: LiPON decomposition reactions with their associated potentials

Figure S3**a** shows the I-V characteristics of 140 nm LiPON layer similar to figure 1 a on a TiN substrate measured at 200K. The clear plateau that was visible in figure 1 a, is no longer present. **b** shows the evolution of the average plateau current versus the layer thickness, current decreases for thinner films. This is the opposite trend of what is expected for electronic leakage, therefore the plateau must be dominated by ionic current.

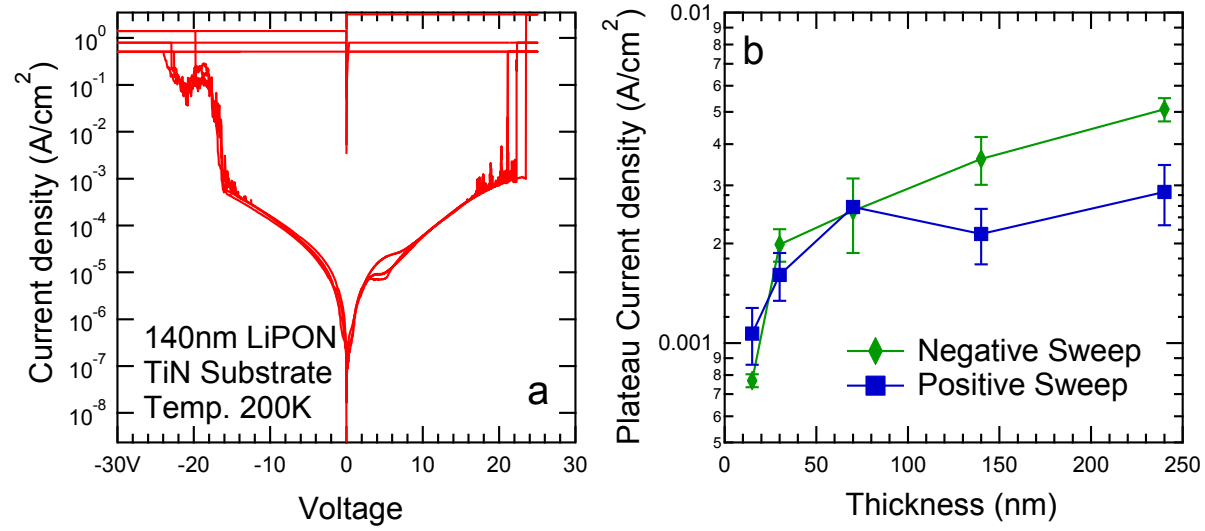

Figure S3a depicts the I-V curves measured at 200K in different dots on a 140 nm LiPON layer using a TiN current collector. A similar characterization, performed at room temperature (300K), was shown in figure 1a. Whereas the latter I-V trace showed a clear constant current plateau, at 200K no plateau is present. This is expected to be due to the limited mobility of the lithium ions at this temperature. Indeed, at 200K, the lithium conductivity will have decreased from the 300K value by roughly 5 orders of

magnitude, down to 10^{-11} S/cm[4]. Therefore ionic transport and thus the buildup of a space charge layer will progress much slower, translating in the absence of a plateau or a reduced current density, as observed (cfr. figure S3a).

The reduced temperature also increases the Gibbs reaction energies. However, the temperature dependence of the decomposition reactions is not linked to the bias polarity as the same decomposition reactions occur, independent of the polarity; The latter only determines at which electrode they proceed. The only effect the reduced temperature has on the Gibbs reaction energy is a possible shift of the potential at which the reactions start. The same holds for the Au-Li alloying reaction that proceeds at higher (negative) potentials when measured at reduced temperature. The presence of symmetry in the breakdown potentials observed at 200K -unlike the 300K case - is due to the slower lithium transport and/or reaction kinetics. At 200K both positive and negative sweep directions result in a breakdown field around 1.5 MV/cm. In the positive sweep direction no influence of the gold-lithium alloy kinetics is expected. Also here the constant current plateau is absent. The disappearance of the plateau as such indicates its close link to Li-ion transport; The change in Gibbs energy is not able to account for the absence of the plateau since hard breakdown is still observed, indicating that enough energy is supplied for the reactions listed above to proceed.

Figure S3b shows the average I-V curve plateau current versus the thickness of LiPON layers on a TiN substrate. A clear trend is present showing higher currents for thicker layers, proving that the plateau current cannot be attributed to electron motion, as electronic leakage current typically decreases with increasing LiPON thickness. When the LiPON layer thickness is reduced below 30 nm, a sudden drop in current is seen. It is expected that from this point on, a significant fraction of the lithium present in the layer can be stored in the gold metal dot or (to a lesser extend) in the native TiO_x. As such a significant increase of the breakdown field is obtained. In such films the formation of a lithium filament becomes increasingly difficult since all the Li-ions generated by the decomposition of the film can be stored in the metal dot. This is described in more detail in the next sections of this work.

[4] Put, B.; Vereecken, P.; Meersschaut, J.; Sepulveda, A.; Stesmans, A. Electrical characterization of ultra-thin LiPON layers for nanoscale batteries. *ACS applied materials and interfaces,* 2015

Material	Ionic conductivity at 25°C
LiPON	$1x10^{-6}$ S/cm [5]
Li_3PO_4	$1x10^{-8}$ S/cm
$Li_4P_2O_7$	$2.3x10^{-7}$ S/cm [6]
$LiPO_3$	$3x10^{-9}$ S/cm [7]

Table T3: Overview of the different ionic conductivities associated with different lithium-phosphate compositions.

[4] Martin, S.; Angell, C. Dc and ac conductivity in wide composition range Li_2O-P_2O_5 glasses, *Journal of non-crystalline solids*, 1986

[5] Yu, X.; Bates, J.; Jellison, G.; Hart, F., A Stable Thin-Film Lithium Electrolyte: Lithium Phosphorus Oxynitride, *Journal of the electrochemical society*, 1997

[6] Pradel, A.; Pagnier, T.; Ribes, M. , Effect of Rapid Quenching on Electrical Properties of Lithium Conductive Glasses, *Solid state ionics*, 1985

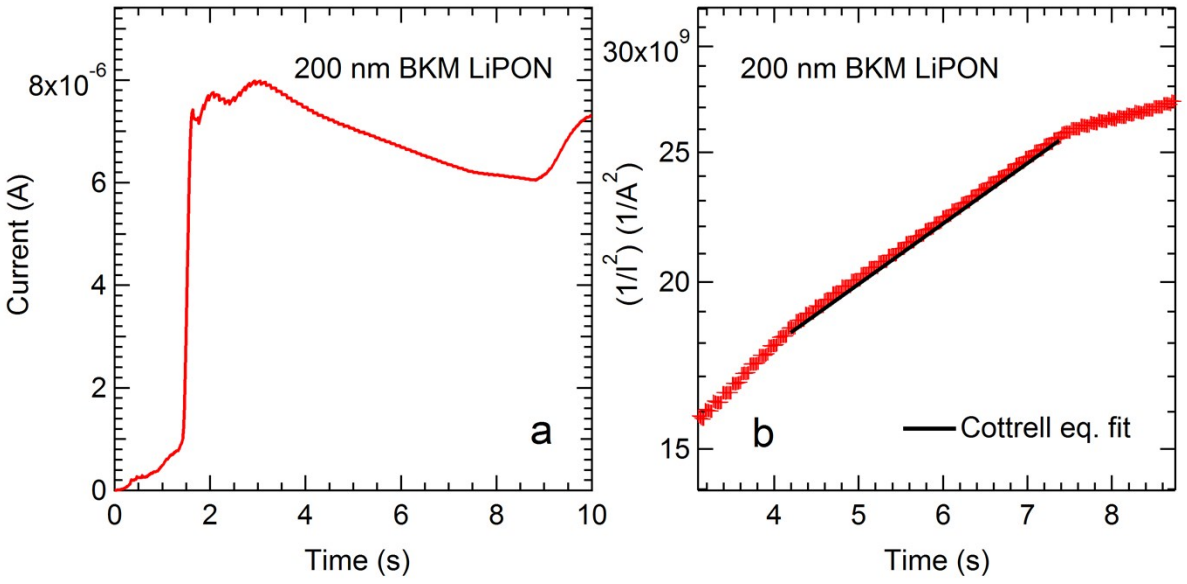

Figure S4 **a** current versus time plot observed on a 200 nm BKM LiPON layer on TiN, contacted using a gold dot with diameter of 500 µm. A linearly increasing potential is applied to the gold dot. **b**) shows a $1/I^2$ vs time plot, a zoom in of the current shown in a, linearized to the Cottrell equation, from where a linear dependence is established. A diffusion constant of 3.10^{-11} cm^2/s can be extracted.